Available online at www.sciencedirect.com
SCIENCE DIRECT®
ELSEVIER
Nuclear Instruments and Methods in Physics Research A 526 (2004) 239–248
NUCLEAR INSTRUMENTS & METHODS IN PHYSICS RESEARCH Section A
www.elsevier.com/locate/nima

A laser pulse shaper for the low-emittance radiofrequency SPARC electron gun

S. Cialdi*, I. Boscolo

University and INFN, via Celoria 16, Milano 20133, Italy

Received 6 August 2003; received in revised form 16 February 2004; accepted 16 February 2004

Abstract

To generate a very low emittance electron beam in a 3-GHz radiofrequency gun, the photocathode has to be driven by a powerful 10-ps light pulse with a rise time of less than 1 ps. This target pulse can be generated from a subpicosecond laser pulse by inserting an appropriate shaping device. We discuss a programmable 4f grating-lens-shaper configured so as to transform a 100-fs pulse emitted by a Ti:Sa laser into a rectangular pulse with a fast rise time. We analyze the sensitivity of the system to perturbations of the optical-component alignment and input-signal characteristics. We then briefly discuss the acousto-optic programmable dispersive filter shaping system.
© 2004 Elsevier B.V. All rights reserved.

PACS: 42.65.Re; 07.05.Tp

Keywords: Low emittance; Rectangular shaping; System sensitivity; Genetic algorithm

1. Introduction

X-ultraviolet (X-UV) free-electron lasers (FELs) [1–3], Compton scattering [4], and the new generation of linear colliders [5] require a low-emittance (a few π mm mrad) electron beam. Numerical calculations for the SPARC [1] (sorgente pulsata e amplificata di radiazione coerente) FEL experiment have shown that the e-beam should have an emittance of $\approx 1\,\pi$ mm mrad [6]. Hence, a radiofrequency (RF) electron gun with a photocathode driven by a powerful 10-ps rectangular light pulse with a fraction of 1 ps rise time has to be implemented. Experimental tests reported in Ref. [7] showed that the e-beam emittance depends on the temporal laser pulse characteristics and that its minimum is reached with a rectangular pulse. A pulse with a rectangular profile is produced by using a shaping system to manipulate a subpicosecond Gaussian-like laser pulse. The schematic of a laser system for photoelectron generation, incorporating a so-called 4f setup as shaper, is shown in Fig. 1. In the scheme, we have chosen to place the shaper between the oscillator and the amplifiers. A continuous-wave Ti:Sa oscillator generating 100-fs pulses with a frequency of 73.9 MHz is proposed for the SPARC project.

The technology for manipulating sub-picosecond pulses in order to generate ultrafast pulses according to user specifications has already been

*Corresponding author.
E-mail address: simone.cialdi@mi.infn.it (S. Cialdi).

0168-9002/$ - see front matter © 2004 Elsevier B.V. All rights reserved.
doi:10.1016/j.nima.2004.02.035

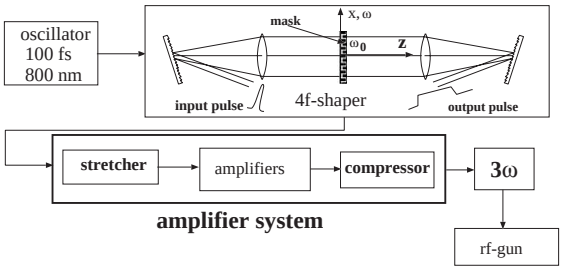

Fig. 1. System layout with the pulse shaper insertion.

developed [8–11]. Pulse-shaping systems have had a strong impact as experimental tools because they provide unprecedented control over ultrafast laser waveforms for ultrafast spectroscopy, nonlinear fiberoptics, and high-energy field physics. We exploit this technology in order to stretch a short pulse into a long pulse with a rectangular shape and a very short rise time.

The principle of pulse shaping is based on the spectral and amplitude modulation of the pulse spectral components. The shaping systems proposed so far with fair success are [9] (i) the liquid crystal programmable spatial light modulator (LCP-SLM); (ii) the acoustic-optic modulator programmable spatial light modulator (AOM-PSLM) [12]; (iii) the acousto-optic programmable dispersive filter (AOPDF) [10,11] and (iv) movable mirrors (MMs) and deformable mirrors (DMs) [9]. The LCP-SLM, used in the majority of experiments, and the first choice for our project, is dealt with in detail in this paper. The AOPDF, interesting for its simple insertion and configuration and programmed for testing in our experiment, is only briefly discussed. The two shapers are based on different physics processes and, thus, different technologies. The design parameters of the LCP-SLM are discussed in view of the system sensitivity to perturbations of the optical-component alignment and input-signal characteristics.

2. General considerations on pulse shaping

The field of a light pulse has, in the time and frequency domains, respectively, the expressions

$$E^*(t) = E(t)\mathrm{e}^{\mathrm{i}\omega_0 t} \quad (E(t) = \sqrt{I(t)}\mathrm{e}^{+\mathrm{i}\phi(t)}) \tag{1}$$

$$E(\omega) = \sqrt{I(\omega)}\mathrm{e}^{-\mathrm{i}\Phi(\omega)}. \tag{2}$$

Pulse shaping is a linear filtering process. In the time domain the filter action of the shaper is represented by an *impulse response function* $h(t)$; in the frequency domain the filter action is represented by the Fourier transform $H(\omega)$ of $h(t)$. The output waveform $e_{\mathrm{out}}(t)$ is the convolution of the input waveform $e_{\mathrm{in}}(t)$ and the impulse response function $h(t)$

$$e_{\mathrm{out}}(t) = h(t) * e_{\mathrm{in}}(t). \tag{3}$$

In the frequency domain we can write

$$E_{\mathrm{out}}(\omega) = H(\omega)E_{\mathrm{in}}(\omega). \tag{4}$$

In general, $H(\omega)$ is a function of the type

$$H(\omega) = T(\omega)\mathrm{e}^{-\mathrm{i}\psi(\omega)}. \tag{5}$$

Therefore, the output will be

$$E_{\mathrm{out}}(\omega) = T(\omega)\sqrt{I_{\mathrm{in}}(\omega)}\mathrm{e}^{-\mathrm{i}[\psi(\omega)+\Phi_{in}(\omega)]}. \tag{6}$$

Appropriate amplitude $T(\omega)$ and phase $\psi(\omega)$ modulations can lead to any kind of output signal. However, when the demand is limited to the temporal intensity profile only, as in the case of RF guns, a phase-only modulation can be applied. In fact, the time domain intensity (and amplitude) is specified, but the temporal phases are free. Phase-only modulation is particularly suitable for operation with very powerful light pulses. In fact, a very powerful pulse is obtained by high amplification, which is accomplished by the sequence of pulse stretching, amplification and, finally, compression [8]. The stretching must be long enough (thus the need for a large spectrum) to avoid strong non-linearities and optics damage. Indeed, photoelectron generation in RF guns requires a huge energy per pulse to obtain the typical nano-Coulomb charge per pulse.

2.1. Linear phase modulation for squaring a Gaussian-like signal

To provide some insight into the problem, let us consider the significant case of linear spectral modulation (i.e., the AOPDF system)

$$\tau(\omega) = \frac{\mathrm{d}\Phi(\omega)}{\mathrm{d}\omega} = b\omega \tag{7}$$

where $\tau(\omega)$ is the frequency-dependent time delay. In the above assumption the phase function is

$$\Phi(\omega) = \int_0^{\omega} b\omega \, d\omega = \frac{1}{2} b\omega^2. \quad (8)$$

The output signal, given by the backward-Fourier transform, has the expression

$$E_{out}(t) = \frac{1}{2\pi} \int_{bandwidth} \sqrt{I_{in}(\omega)} e^{-i(b/2)\omega^2} e^{i\omega t} \, d\omega. \quad (9)$$

The spectral bandwidth of 30 rad/ps around the central frequency is considered in the calculations (Fig. 2). The spectral components within that region cover more than 70% of the pulse energy. A simple linear time delay curve over the whole frequency domain leads to an output pulse with too long a rise time (1b in Fig. 2). A stepwise curve (2a in Fig. 2) leads to fast leading and trailing edges (as a result of the superposition of many spectral components in phase), which have, however, overshoots that are too high. The wider the flat lateral segments, the faster the rise time, but also the higher the overshoots. Removal of the overshoots requires amplitude reduction of the relative spectral components (3a in Fig. 2). The output signals are simply obtained by applying the Fourier transform as written in Eq. (9). The signals are rather spiky because of the discontinuities both of the phase and of the transmission functions. We will not deal with the problem further, because the aim of the calculation here is mainly tutorial.

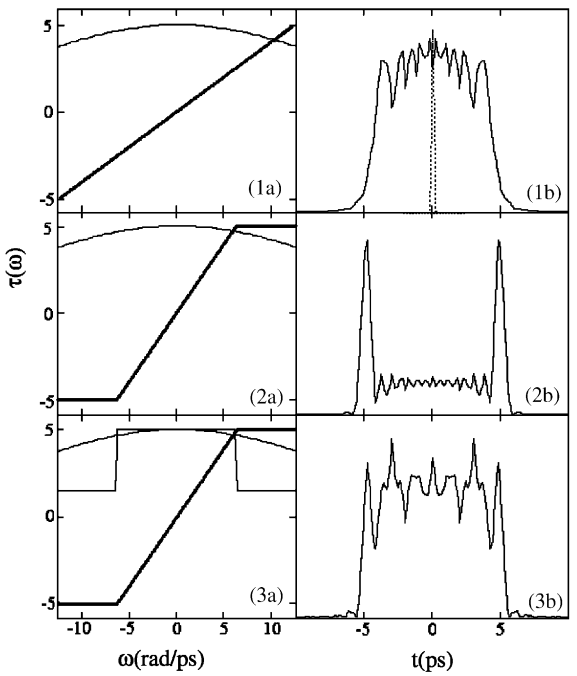

Fig. 2. Left frames: The time delay $\tau(\omega)$ functions (bold lines) and the section of the Gaussian spectrum (thin curved lines) used for the calculations. Frame 3a also shows the step variation at the two sides of the transmission function. Right frames: Numerical calculated output pulses relative to the different τ curves shown in the left frames. The amplitude modulation of the transmission function leads to removal of the overshoots.

3. LCP-SLM system

We now discuss the operating principles of the system, the computer program developed for the simulations and the sensitivity of the output pulse configuration to perturbations of the optical-component alignment and input-signal characteristics.

3.1. System operation

The optical components of a 4f setup are two gratings, two lenses placed at the focal distances, and a filter mask placed at the centre of the system (Fig. 1). The system is a zero time-dispersion line. The physical operations performed by the device in the filtering process are (a) transformation of the input signal into a fan of spectral components by means of a grating; (b) transformation of the

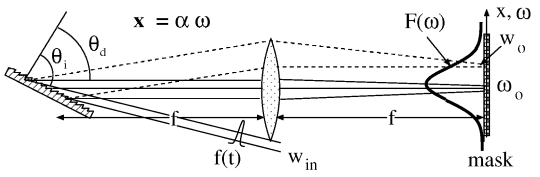

Fig. 3. Input θ_i and diffracted θ_d. The mask and the grating are at a distance f from the lenses. The Gaussian Fourier spectrum is shown at the mask. The spectral components of the input light beam are separated by the grating and focused at the mask by a lens with a beam waist w_0.

component fan into a comb of thin rays with a spot size w_0, by means of a lens (Fig. 3); (c) modulation, in either amplitude or phase, or in both, of the spectral components by a modulating mask; (d) the reverse operation of transforming the comb rays into a convergent beam by a second lens and (e) re-combination of the components into a signal by a second grating. The light polarization at the grating is perpendicular to the polarization required by the mask, hence a waveplate for 90° polarization rotation is inserted in between. The output pulse profile is given by the Fourier transform of the pattern transferred by the mask onto the spectrum.

The mask of an LCP-SLM system is an array of pixels interleaved with small gaps (Fig. 4). The mask chosen for the SPARC project is the Jenoptik model SLM-S 640/12 mask (JENOPTIK Laser, Optik, System GmbH, Jena, Germany). The dimensions of the pixels and gaps are, respectively, 97 and 3 μm wide, and the number of pixels is 640.

In a first approximation, the spectral dispersion follows a linear law

$$x \simeq \alpha\omega. \tag{10}$$

The frequency ω refers to the central frequency ω_0 of the spectral domain spanned by the signal. The

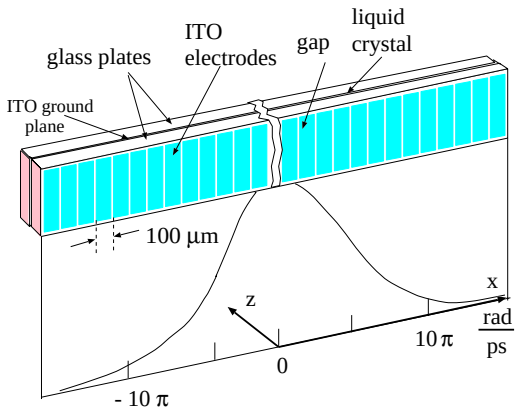

Fig. 4. Schematic of an electronically addressed LCP-SLM. A thin layer of nematic liquid crystal is sandwiched between two pieces of glass, whose inside surfaces are coated with a thin, transparent, conducting film of indium tin oxide patterned as an array of pixels.

filter function $H(\omega)$ is related to the physical transmission function of the mask. The field just behind the mask, with $H_{\mathrm{SLM}}(x)$ the physical transmittance of the mask, is given by

$$E_{\mathrm{out}}(x,\omega) \sim H_{\mathrm{SLM}}(x)\, \mathrm{e}^{-(x-\alpha\omega)^2/w_0^2}\, E_{\mathrm{in}}(\omega). \tag{11}$$

Note that the field behind mask will generally be an envelope of many Hermite–Gaussian modes. However, it is possible to put a mode filter inside the apparatus that cuts out all the modes but the lowest TEM_{00} [13]. The filter function $H(\omega)$ of Eq. (4) will have the coefficient of that lowest mode. The filter function, after Eq. (11) and the above assumption, will be

$$H(\omega) = \sqrt{\frac{2}{\pi w_0^2}} \int_{\mathrm{mask}} H_{\mathrm{SLM}}(x)\, \mathrm{e}^{-2(x-\alpha\omega)^2/w_0^2}\, \mathrm{d}x. \tag{12}$$

The effective filter function is the convolution of the mask-pattern function with the pulse intensity profile. As the mask is pixellated, so is the filter function $H_{\mathrm{SLM}}(\omega)$ of the mask. Eq. (3) is changed into [14]

$$e_{\mathrm{out}}(t) \cong \left[\sum_n h\left(t - n\frac{1}{\delta\nu}\right) * e_{\mathrm{in}}(t)\right] \frac{\sin(\pi\delta\nu t)}{\pi\delta\nu t}. \tag{13}$$

The spectral width $\delta\nu$ is relative to the bandwidth collected by each pixel of width $\delta x (\delta\nu = \delta x/2\pi\alpha)$. Negligibly small interpixel gaps and $2w_0 < \delta x$ are assumed for obtaining expression (13). Pixellation produces an output pulse, which is the convolution of the input pulse not only with the desired impulse response function $h(t)$, but also with a series of replica impulse response functions, $h(t - n\delta\nu^{-1})$, occurring at times $t = n\delta\nu^{-1}$. The whole result is weighted by a temporal window function, $\sin c(\pi\delta\nu t)$, which has the first zeros at $t = \pm\delta\nu^{-1}$. However, for our objective, which is to obtain a rectangular pulse intensity after frequency multiplication, we can argue that the lateral replica will become negligible with respect to the main pulse.

3.2. System configuration

3.2.1. Grating and spatial dispersion

The system configuration is largely determined by the angular dispersion α of the spectral

components and is related to the system parameters by

$$\alpha = \frac{\lambda_0^2 f}{\mathrm{d}2\pi c \cos[\theta_\mathrm{d}(\lambda_0)]}. \tag{14}$$

In the above equation, f is the focal length, λ the wavelength, c the speed of light, θ_d the diffracted angle of the central frequency (Fig. 3). The equation comes from the grating law $m\lambda = \mathrm{d}(\sin\theta_\mathrm{i} + \sin\theta_\mathrm{d})$ with $m = 1$. As we want efficient diffraction into the first order, for good spectral separation the grating period d should be as small as possible. The grating presented in brochures as having 2000 grooves/mm ($d = 0.5$ μm) can provide the required dispersion of a few centimeters, at a distance of about half a meter for a 100-fs pulse with a carrier wavelength of 800 nm.

The dispersion α remains fixed by the mask dimension Δx and the spectral bandwidth $\Delta\omega$ selected for the system, since $\alpha = \Delta x/\Delta\omega$. With the selected spectral portion of $\Delta\omega = 30\pi$ rad/ps we get $\alpha = 0.68$ mm ps/rad. Once α is fixed, Eq. (14) relates the focal length to the input angle (Fig. 5a). We looked at the variation in α with θ_i, (Fig. 5b), to get a trade-off between the focal length and the input angle, so as to have a sufficiently low sensitivity of α to θ_i perturbations, combined with reasonable apparatus dimensions (that is a focal length). We propose a focal length $f = 700$ mm and, consequently, an input angle $\theta_\mathrm{i} = 62.76°$.

3.2.2. Mask and beam waist

The response function from Eq. (12), taking into account the finite number of pixels and the finite dimensions of the beam waist w_0, is

$$H(\omega) = \sqrt{\frac{2\alpha^2}{\pi w_0^2}}\, H_\mathrm{SLM}(\omega) * \mathrm{e}^{-2(\alpha^2/w_0^2)\omega^2}. \tag{15}$$

We have already seen that the filter function $H_\mathrm{SLM}(\omega)$ is step-shaped. The steps are smoothed by convolution with the Gaussian envelope function $\mathrm{e}^{-2\,\alpha^2\omega^2/w_0^2}$ originated by the Gaussian spot of each spectral component at the mask. To conserve good spectral resolution (essential for a long flat pulse), the beam waist must be well below the pixel dimensions.

Taking the output pulse as a function of different beam waists, we ended up with a beam waist of $w_0 = 20$ μm [15]. This value seems feasible for the chosen focal length and the foreseen input spot size. The beam waist w_0 after simple calculations is

$$w_0 = \frac{\cos\theta_\mathrm{i}}{\cos\theta_\mathrm{d}} \frac{\lambda f}{\pi w_\mathrm{in}} \tag{16}$$

where w_in is the waist of the input beam at the grating. Having fixed all the parameters but the input waist, this w_in is 5.8 mm.

As for the choice of the spectral bandwidth $\Delta\omega$, note that the frequency interval $\Delta\omega$ is relevant to the rise time and plateau roughness of the rectangular pulse and also to the shaper dimensions. The bandwidth of 30 π rad/ps comes from a

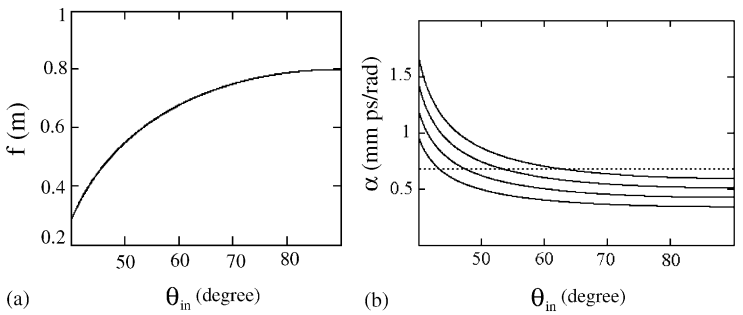

Fig. 5. (a) Curve of the focal length as a function of the incident angle. (b) Angular deviation as a function of the incident angle θ_i for different focal lengths (in order from the top 700, 600, 500 and 400 mm). A trade off between θ_i and f must be done: the longer the focal length the lower the sensitivity to θ_i perturbation. As low sensitivity is needed, θ_i must be greater than 50°. The dotted line in (b) represents the possible incident angles for α slowly varying with angle.

trade-off among the three requirements of fast rise time, flat plateau and reduced mechanical dimensions.

3.3. A numerical program for phase-only filtering

By choosing phase-only filtering and a beam waist w_0 smaller than the pixel dimensions, the spectral amplitudes remain substantially unchanged in crossing the system. Thus, we can write $H_{SLM}(\omega) = \exp[-i\psi(\omega)]$. An analytical calculation for H_{SLM} does not exist, but many numerical solutions are available. We discuss a computer-assisted calculation capable of providing a response function H_{SLM} that gives an output pulse fairly well approximating the target pulse. A specific numerical program (in C++ language) was developed.

The transfer function is calculated with an iterative procedure: The spectral patterned function is updated according to a genetic stochastic optimization algorithm (GA) [16,17]; the convolution of the updated transfer function with the signal of the previous cycle provides a new output signal; a *cost function* is calculated with the new signal; if this updated *cost function* is lower than the *cost function* of the previous cycle, the updated spectral patterned function will be accepted; otherwise, it will be rejected and a new cycle starts with a fresh spectral pattern function. The iterations are stopped when the value of the *cost function* arrives at saturation. The final phase pattern $\Phi(\omega) + \psi(\omega)$ is transferred to the mask. The complex spectral field $E(\omega)$ of the input pulse, i.e., its spectral amplitude $A(\omega)$ and phase $\Phi(\omega)$), and the temporal amplitude $E_{target}(t)$ of the target pulse are given as inputs. The initial trial phase vector Φ has all the phases at the pixels set at zero value. In each iteration a random phase change $\delta\psi_i$ is generated according to $\delta\Phi_i = R$, where R is a random variable uniformly distributed in the interval -0.5 to $+0.5$. The index i refers to the ith pixel. The calculation procedure is illustrated schematically in Fig. 6. There are many types of *cost functions* and the choice is determined by the particular target function [17,18]. In our case of a long rectangular pulse, the choice of the *cost function* is very important [15]. We compared the qualities of the output pulse profile, in terms of plateau flatness, obtained with the following *cost functions*: $C_1 = \sum_k |I_k - I_k^{target}|$; $C_2 = \sum_k (I_k - I_k^{target})^2$; $C_3 = \sum_k [I_k^2 - (I_k^{target})^2]$ and $C_4 = \sum_k |I_k - I_k^{target}|^3$. The *cost function* C_2 proved to be the best for the task. The index k in the above equations indicates the kth section of the segmented function. The pulse profile shown in Fig. 7 was obtained with the program. The rise time is about 0.5 ps, the flatness is quite good and the lobes at the sides are very small. These side lobes disappear at the third harmonic, that is, calculating the intensity as the cube of the fundamental I^3 (Fig. 7b). The relation between the first and the third harmonic is a fairly crude way of looking at

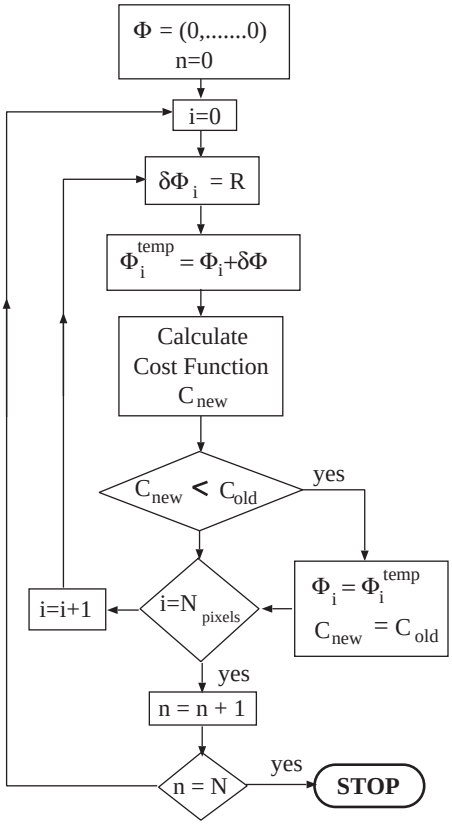

Fig. 6. Adaptive algorithm: The inverse Fourier transform is applied to obtain the output waveform at each iteration of the genetic algorithm; the output and target waveforms are then compared. The index N, the number at which the iteration is stopped, is fixed by the value of the *cost function* at saturation.

the problem. In fact, the first-harmonic rectangular pulse crosses two amplifiers before entering the crystal for the third-harmonic generation. Nonetheless, since the non-linearity strongly exalts the amplitude modulations present in the signal, the reported result should be realistic. In simulations of the SPARC experiment, amplitude oscillations up to about 30% seem acceptable [19]. Therefore, the phase-only modulation leads to a satisfactory rectangular output pulse, as the plateau roughness is only a few percent and the rise time less than 1 ps.

We investigated via simulations the system sensitivity to variations in the input pulse length, the dispersion (incident angle) and the input pulse profile. The sensitivity of the shaper to perturbations depends on the spectral acceptance, once the type of modulation has been fixed. In fact, we verified that the wider the spectral acceptance, the higher the system sensitivity to any variation, but also the smoother the pulse flatness at the optimized filter pattern. A pulse lengthening of a couple of femtoseconds leads to a 10% increase in roughness. It could be advisable to choose a smaller portion of the spectral bandwidth and, hence, accept a lower flatness in order to obtain a lower sensitivity to pulse-length deviations. The increase in plateau roughness because of perturbation of the spatial dispersion (due to the variation in the incident angle) is shown in Fig. 8: its variation with $\Delta\alpha/\alpha$ is slow. The reason for the output change is that a variation in α produces a variation in the spectral components hitting the mask pixels. This leads to a spectral phase pattern that is no longer optimized for a flat output.

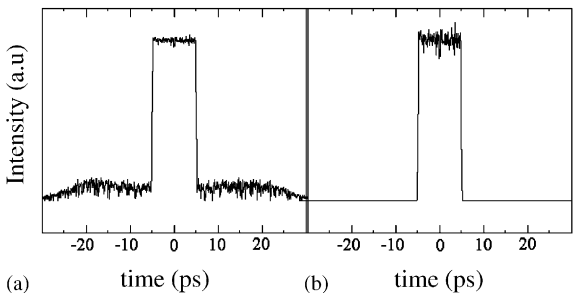

Fig. 7. Simulated output pulses after the shaper obtained with the iterative algorithm: The signals in (a) and (b) refer to the fundamental harmonic and third harmonic, respectively. This harmonic intensity is simply calculated by the third power of the fundamental harmonic I^3.

It is apparent from Fig. 8b that, accepting an enhancement of the roughness of up to 30%, the acceptable extent of the α variation is 2%. Note that the variation is not left–right symmetric about the centre. The parametric curves reported in Fig. 9 present the percentage variation of α at the different input angles. The parameter of the curves is the percentage variation of the input angle as indicated in the figure. The line $\Delta\alpha/\alpha = 2\%$ shows that the allowed variation of the input angle is about 2% at the chosen $\theta_i \simeq 63^\circ$. This perturbation of the input angle can be easily controlled in an optic system.

To round off, we also performed simulations with the iterative Fourier transform (Gerchberg–Saxton) algorithm [20]. The simulated signal-

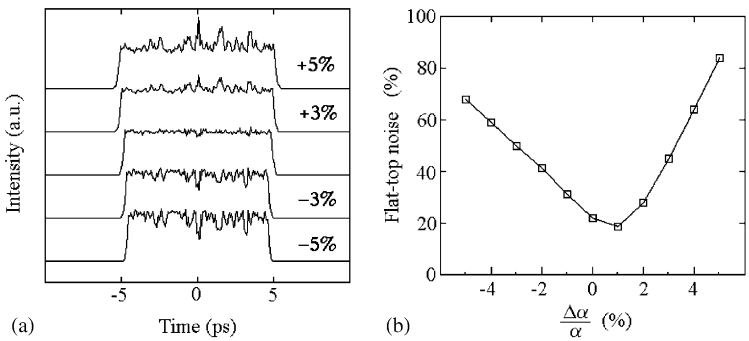

Fig. 8. (a) Variation of the signal plateau flatness at the third harmonic for different values of $\Delta\alpha/\alpha$. (b) A 20% enhancement of the plateau roughness occurs for an angular dispersion variation of about 2%. The flat-top noise was calculated by $(I_{max} - I_{min})/I_{average}$.

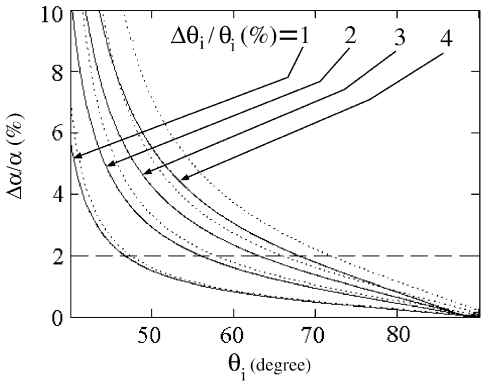

Fig. 9. Sensitivity of dispersion α vs. input angle θ_i at a fixed focal length of 700 mm. Continuous lines: percentage variations of 4%, 3%, 2% and 1%, respectively. Dotted lines: negative variations in θ_i. Note that $\Delta\alpha/\alpha$ is not symmetric with respect to the two side variations and also that $\Delta\alpha/\alpha > 0$ when $\Delta\theta_i < 0$ and vice versa.

output was notably worse than that obtained with our program based on the genetic algorithm.

4. The AOPDF system

Here, we briefly look at the basic principles of operation and the advantages and disadvantages of an AOPDF device. More information about the AOPDF can be found in Refs. [10,11] and, for the other types of shapers, in the review paper [9].

The AOPDF (also known as DAZZLER) is based on collinear acousto-optic interaction in a tellurium dioxide (TeO_2) crystal (acousto-optic modulator, AOM). The crystal is driven by an RF signal, which generates a propagating acoustic wave that sets a spatial wave in the crystal and consequently a refractive index grating via the photoelastic effect. The grating period is $K = v_{ac}/\Omega$, where Ω and v_{ac} are, respectively, the frequency and the velocity of the wave. Each spectral component of the input pulse, in its propagation along the ordinary axis, is diffracted into an output pulse propagating along the extraordinary axis at a point $z(\omega)$ of the crystal (Fig. 10), where the resonance conditions

$$k_2 \simeq k_1 + K, \quad \omega_2 \simeq \omega_1 + \Omega \tag{17}$$

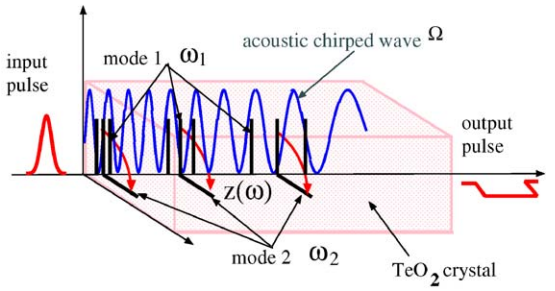

Fig. 10. Schematic of the AOPDF principle. The acoustic wave and the optical incident and diffracted waves are collinear and propagating along the z-axis. The components of the acoustic, incident and diffracted waves match the resonance conditions at different values of the z coordinate, as indicated by the arrows.

are matched. In the above equation, k_1 is the incident wavenumber; k_2, the diffracted. The frequencies of the two optical waves are approximately equal. As the spectral diffraction occurs at different distances, each component will cross the crystal length L in a different time $\Delta t(\omega)$, proportional to the length $z(\omega)$. The system behaves like a dispersive system, where the group-velocity $v_g(\omega)$ has a significant value.

The TeO_2 crystal of the AOPDF has a typical 2.5−3 cm length in a quasi-collinear configuration. At $\lambda = 800$ nm, the refractive indexes for the two ordinary and extraordinary waves are, respectively, $n_1 = 2.226$ and $n_2 = 2.374$. The dispersion of the frequencies from 700 to 900 nm requires an RF frequency range between 40 and 60 MHz.

Amplitude modulation (besides phase modulation) can be obtained simply by modulating in amplitude the RF-driving signal. The diffraction efficiency is a function of acoustic intensity.

Its compactness, simple insertion and the availability of both phase and amplitude modulations make the Dazzler very attractive. However, it has some disadvantages. It does not allow a long crystal because of low efficiency in RF signal transmission, so long longitudinal dispersion is impossible. Non-linearities already appear at medium acoustic wave power, which prevents efficient diffraction. Furthermore, matching of the transducer impedance is difficult. Although these disadvantages make the AOPDF less attrac-

tive than the LCP-SLM device, both are going to be considered for the SPARC project: the LCP-SLM for its reliability and flexibility, the AOPDF for its simplicity.

4.1. A short note on the AOM-PSLM shaping system

An AOM crystal with the refractive index grating described above can be set perpendicular to the propagation axis in a 4f system, in substitution of the liquid crystal mask. The apparatus is named AOM Programmable SLM (AOM-PSLM). The spatially dispersed spectral components are diffracted by the grating, which is locally tuned to the components. The tests showed the appearance of acoustic nonlinearities at a lower RF power level than needed for high diffraction efficiency [9]. The disadvantages with respect to the LCP-SLM system leads almost naturally to choice of this second system.

5. Conclusions

A 4f spatial light modulator with a programmable mask, phase-only patterned, seems appropriate for the task of producing a 10-ps target pulse with a rise time of less than 1 ps. The Jenoptik model SLM-S 640/12 mask, used in the numerical tests, proved capable of producing the required rectangular pulse with a 100-fs input pulse. The spectral pattern for the phase mask was obtained with the use of a home-made numerical program based on a genetic stochastic optimization algorithm. Phase-only pulse shaping is capable of maintaining the rise time of the input pulse. This result indicates that the input driving pulse could be wider than the 100 fs used in the calculations. The shaper has sufficient flexibility to recover the distortions introduced into the pulse profile by the amplifiers of the laser system. The mask pattern can be changed in a relatively simple way, which makes the device flexible for adapting the transfer function to changing user requests, such as passing from a rectangular pulse to a ramp pulse shape. The LCP-SLM system has relatively low sensitivity to perturbation of the input angle, while the sensitivity is high for mask alignment. Operation of the laser system at the third harmonic, as required by the photo-electron process, has the beneficial effect of lowering any possible side lobe, but has also the negative effect of enhancing the amplitude modulation of the flat-top.

Acknowledgements

The work is partly supported by MIUR, *Progetti Strategici*, DD 1834, December 4, 2002.

References

[1] SPARC Conceptual design of a high-brightness linac for soft X-ray SASE FEL source, EPAC 2002, La Villette, Paris, 5 June 2002.
[2] M. Cornacchia, et al., Linac coherent light source (LCLS) design study report, Report No. SLAC-R-521/UC-414, revised 1998, Stanford University, Stanford, CA.
[3] F. Richard, et al., TESLA, the superconducting electron-positron linear collider with an integrated X-ray laser laboratory, technical design report, Desy Report No. DESY2001-011, DESY, Hamburg, 2001.
[4] P.T. Springer, et al., Ultrafast material probing with the Falcon/Linac Thomson X-ray Source, LLNL proposal 01-SI-007, 2002.
[5] J. Yang, M. Washio, A. Endo, T. Hori, Nucl. Instr. and Meth. A 428 (1999) 556.
[6] M. Ferrario, M. Boscolo, V. Fusco, C. Vaccarezza, C. Roncisvalle, J.B. Rosenzweig, L. Serafini, in: ICFA Workshop The physics and application of high brightness electron beams, Chia Laguna, Sardinia, Italy, 1–6 July 2002.
[7] J. Yang, F. Sakai, T. Yanagida, M. Yorozu, Y. Okada, K. Takasago, A. Endo, A. Yada, M. Washio, J. Appl. Phys. 92 (2002) 1608.
[8] S. Backus, C.G. Durfee III, M.M. Murname, H.C. Kapteyn, Rev. Sci. Instrum. 69 (1998) 1207.
[9] A.M. Weiner, Rev. Sci. Instrum. 1 (2000) 1929.
[10] P. Tournois, Opt. Commun. 140 (1997) 245.
[11] F. Verluise, V. Launde, J-P. Huignard, P. Tournois, A. Migus, J. Opt. Soc. Am. B 17 (2000) 138.
[12] M.R. Fetterman, D. Goswami, D. Keusters, W. Yang, J.K. Rhee, W.S. Warren, Opt. Lett. 23 (1998) 1843.
[13] R.N. Thurston, J.P. Heritage, A.M. Weiner, W.J. Tomlinson, IEEE J. Quantum Electron. 22 (1986) 682.
[14] M.M. Wefers, K.A. Nelson, J. Opt. Soc. Am. B 127 (1995) 1343.

[15] S. Cialdi, I. Boscolo, A. Flacco, Features of a phase-only shaper relative to a long rectangular ultraviolet pulse, J. Op. Soc. of Am. B, accepted.
[16] D. Meshulach, D. Yelin, Y. Silberberg, Opt. Commun. 138 (1997) 345.
[17] D. Meshulach, D. Yelin, Y. Silberberg, J. Opt. Soc. Am. B 155 (1998) 1615.
[18] A.M. Weiner, S. Oudin, D.E. Leaird, D.H. Reitze, J. Opt. Soc. Am. B 105 (1993) 1112.
[19] D. Alesini, et al., Status of the beam dynamics studies for the SPARC Project, SPARC-BD-03/001, d note, Lab. Naz. Frascati-LNF, Italy.
[20] M. Hacker, G. Stobrawa, T. Feurer, Opt. Express 9 (2001) 191.